Waste Management 169 (2023) 125–136

Contents lists available at ScienceDirect

Waste Management

journal homepage: www.elsevier.com/locate/wasman

Research Paper

Role of acidic hydrochar on dechlorination of waste PVC in high temperature hydrothermal treatment and fuel properties enhancement of solid residues

Vahab Ghalandari [a], Maurizio Volpe [b], Fabio Codignole Lùz [b], Antonio Messineo [b], Toufiq Reza [a,*]

[a] Department of Biomedical and Chemical Engineering and Sciences, Florida Institute of Technology, 150 West University Boulevard, Melbourne, FL 32901, USA
[b] Faculty of Engineering and Architecture, University of Enna, Kore, viale delle Olimpiadi snc, 94100 Enna, Italy

ARTICLE INFO

Keywords:
Acidic hydrochar
Dechlorination
Hydrothermal treatment
Slagging and fouling indices
Solid fuel
Waste plastic

ABSTRACT

In this study, the chlorine mitigation from waste polyvinyl chloride (WPVC) during high temperature co-hydrothermal treatment (co-HTT) and the properties of the generated solid products were assessed. WPVC was co-fed with acidic hydrochar (AHC), which was produced via hydrothermal carbonization of pineapple waste in the presence of citric acid water solution. High temperature co-HTT experiments were performed at 300–350 °C, 0.25–4 h of reaction time, and 0–20 wt% AHC loading. Co-HTT solid products (co-HTT_SP) were characterized via proximate analysis, ultimate analyses, combustion analysis, and ash analysis. The results show that the addition of 5% AHC enhances the dechlorination efficiency (DE) of WPVC from 89.35% to 97.66% at 325 °C and 0.5 h. The highest DE, reaching 99.46%, was achieved at 350 °C and 1 h in the presence of 5 wt% AHC. Furthermore, loading 5% AHC improved the higher heat value (HHV) of the solid products from 23.09 to 31.25 MJ/kg at 325 °C and 0.5 h. The maximum HHV (34.77 MJ/kg) of a solid product was achieved at 350 °C, 4 h, in the presence of 5 wt% of AHC. The co-HTT solids shown low slagging indices, fouling indices, alkali indices, and medium chlorine contents. These findings support the viability of WPVC conversion into clean solid fuel via co-HTT.

1. Introduction

Polyvinyl chloride (PVC) is one of the most widely utilized thermoplastics in terms of global polymer usage (Sadat-Shojai and Bakhshandeh 2011). PVC has become a ubiquitous polymer as a result of its cheap cost and great performance, as well as the vast variety of products that may be created from varied processing conditions and procedures (Garcia et al. 2006; Yarahmadi, Jakubowicz, and Martinsson 2003; Braun 2001). Even though PVC products have a long useful life and there is a significant lag between PVC production and disposal, which results in a net accumulation of waste PVC (WPVC) (Slapak, van Kasteren, and Drinkenburg 1999; M. K. Patel et al. 1998; M. Patel et al. 2000). In fact, the disposal of WPVC has already become a public concern (Nakamura et al. 2009; Garcia et al. 2007; Burat, Güney, and Olgaç Kangal 2009; Braun 2002). WPVC disposal in landfill or incineration of WPVC face some major challenges. For example, the leaching of phthalate and heavy metals like lead, cadmium, and tin, which are components of stabilizers, may be problematic in landfilling (Sato et al. 1998). The incineration produces hazardous pollutants and a large quantity of hydrochloric acid, which induce corrosion in the furnace and release trace quantities of other hazardous gases, resulting in serious environmental issues (Sato et al. 1998). To overcome these issues, a sustainable WPVC disposal system is required.

Hydrothermal treatment (HTT) has recently been presented as a viable approach for the dechlorination of PVC (Yoshioka et al. 2008; X. Ma et al. 2015; Poerschmann et al. 2015). HTT refers to the process of treating materials in water at a certain temperature and pressure in order to maintain the water in either a subcritical or supercritical condition in order to degrade organic compounds (Bermejo and Cocero 2006; Kritzer and Dinjus 2001; Lavric et al. 2005). HTT is a process which involves reactions in homogeneous media, has the benefit of quick response rate (Yu et al., 2016a), and has been successfully employed in the process of resource recovery as well as the treatment of hazardous wastes like PVC (Benavente, Fullana, and Berge 2017; Yu

* Corresponding author.
E-mail address: treza@fit.edu (T. Reza).

https://doi.org/10.1016/j.wasman.2023.07.005
Received 6 April 2023; Received in revised form 8 June 2023; Accepted 3 July 2023
Available online 7 July 2023

et al., 2016b). For instance, Endo and Emori (Yoshioka et al. 2008) carried out research on the high-temperature decomposition of PVC at high pressure, and they observed that the DE approached to 100% at 300 °C at 19.3 MPa. According to Lu et al. (J. Lu, Ma, and Gao 2002), the DE was 95% at 240 °C after a two hours treatment in an alkaline environment, and reached 100% after 15 h at the same temperature. According to Takeshita et al. (Takeshita et al. 2004), during the HTT DE of WPVC, the chlorine was mostly released as HCl, which was dissolved in water. HTT of WPVC carried out at temperatures between 180 and 260 °C have shown an increasing rate of dechlorination with increasing temperatures (Zhao et al., 2018a). Solid product from HTT of chlorinated organic wastes was shown to have a very low sorption potential, especially for polar organic contaminants, providing strong evidence that it is environmentally beneficial (Zhao et al., 2018a). To improve the dechlorination and degradation of PVC waste, different additives, including NaOH (Zhao et al., 2018b), C_2H_5OH (Xiu et al., 2020a), NH_3 (Xiu et al., 2020b), and urine (Xiu et al. 2023) were introduced. The inclusion of NaOH and NH_3 increased the efficiency of PVC dechlorination to 95% and 98.7% at a temperature of 300 °C, respectively (Xiu et al., 2020a; Xiu et al., 2020b). In general, HTT of WPVC with higher HTT temperature and modified pH resulted in higher DE.

Co-treatment of plastic and biomass has been generating tremendous interest recently, as it poses significant advances compared to standalone treatment (Uzoejinwa et al. 2018; Wu et al. 2017; Hongthong et al. 2020). Because the temperature ranges of thermal breakdown for plastic and biomass overlap, thermochemical co-processing is conceivable (Jakab, Várhegyi, and Faix 2000). For instance, Zhou et al. (Zhou et al. 2015) observed that pyrolysis of biomass with PVC boosted char output as well as CO and CO_2 production. PVC-derived intermediates were also observed to improve char output during the co-pyrolysis of PVC and other plastic wastes (Yu et al., 2016a). Co-pyrolyzing PVC and biomass has been proven to minimize HCl emissions when compared to pyrolyzing PVC alone (Braden and Bai 2018). Synergistic effects were observed between PVC and sawdust during co-pyrolysis in another study (Sørum, Grønli, and Hustad 2001). Under pyrolytic conditions, HCl produced from the PVC appeared to act as an acid catalyst, boosting biomass dehydration (Sørum, Grønli, and Hustad 2001). Nevertheless, the residual Cl atoms end up as organic chlorides in the liquid and solid products (Zhou et al. 2015; Kuramochi et al. 2008). Chloride-contaminated liquid phase (pyrolysis-oil), and solid phase (char) can pose serious complications in application (Zhou et al. 2015; Kuramochi et al. 2008). Although co-pyrolysis is common in literature, co-HTT is still scarce. It was reported recently that the solid phase generated by co-HTT of PVC and lignin might be used as a non-toxic solid fuel because HCl is water soluble (Shen 2016). However, when PVC is co-converted with other organic components like cellulose, dehydrochlorination is less successful, according to their findings (Shen 2016). It has been reported that adding liquid acid as catalyst can improve the co-HTT of PVC in terms of chlorine removal from PVC and the production of a solid residue with higher HHV (X. Lu et al. 2020; Wei et al. 2022). However, in many industrial chemical processes, solid acids are preferable over liquid acid catalysts due to their advantages of strong acidity, ease of separation, minimal corrosion potential, and superior recyclability (Liu and Liu 2020; Chen et al. 2019; Corma 1997). In terms of environmental responsibility, the production of solid acid catalysts from renewable biomass has major strategic repercussions to consider (Liu and Liu 2020). Our group, recently successfully produced an AHC from pineapple using HTT within the presence of citric acid (Volpe et al. 2021).

This research aimed to examine the influence of mentioned AHC on the dechlorination of WPVC through the co-HTT. Experiments were conducted to determine the influence of reaction temperature, reaction time, and AHC loading on DE. Ultimate analysis, proximate analysis, higher heating value, chemical alteration, chlorine migration, and ash properties were studied for the Co-HTT solid products (co-HTT_SP). The present study reports an innovative approach shading light in the capability of AHC toward dechlorination of WPVC opening a way of producing an environmentally safe solid fuel from WPVC by co-HTT.

2. Material and methods

2.1. Material

PVC plumbing as a WPVC was purchased from a local supplier. A high-grade nitrogen gas (99.9%) was provided from NexAir LLC. (Melbourne, FL, USA). The AHC that had been produced as a result of our most recent work (Volpe et al. 2021) was used in this investigation. AHC was produced by performing HTC on pineapple waste in the presence of citric acid at 220 °C for 1 h. AHC had a total acidic group concentration of 1587.9 mol/g.

Nitric acid with a concentration of 65% and hydrogen peroxide with a 30% concentration, both of the Suprapur grade (Fisher Scientific, Waltham, MA, USA) were used to dissolve WPVC and solid co-HTT products to evaluate for DE. The Milli-Q water purification device (Millipore, Bedford, MA, USA) was utilized to produce deionized and distilled water (DDW), which had the potential of producing 18 MV cm specific resistivity.

2.2. Co-hydrothermal treatment

The co-HTT tests were performed utilizing a Parr Hast-C batch reactor with a capacity of 100 mL (Model: 4560, Moline, IL, USA). Hast-C was used to prevent corrosion during co-HTT (Ghalandari et al., 2022b). The reactor was heated using a ceramic electrical heater at a rate of 5 °C/min. For each test, 4.0 ± 0.1 g of powdered WPVC (size: 1.0 ± 0.5 mm) and a certain quantity of AHC, and a certain volume of deionized (DI) water were added into the vessel of the reactor to obtain a mass ratio of 1:10 of solid (WPVC + AHC) to DI water. Three separate purges with nitrogen gas were performed on the reactor in order to remove oxygen from the headspace. The co-HTT tests were conducted at three temperatures (300, 325, 350 °C), five reaction times (0.25, 0.5, 1, 2 and 4 h), and six AHC loadings ratio (2, 3, 4, 5, 10, and 20 wt%). At the end of the co-HTT reaction, a cold-water bath was used to quickly cool down the reactor to ambient temperature, and a fume hood was used to vent the gaseous byproducts. Solid and liquid phases were recovered via vacuum filtration of the HTT slurry. Solid residue was washed with DI water after phase separation to remove from the solid residue the mother liquors. To determine the solid yield (SY), the following equation was utilized (Tahmid et al., 2021b):

$$\mathrm{SY\ (wt\%)} = \left(\frac{\text{Mass of dried solid after co} - \text{HTT}}{\text{Mass of dried feedstock}}\right) \times 100\% \quad (1)$$

All tests were replicated to reduce the test errors and the standard deviation of the data was reported. As the emphasis of this work was on the yield and quality of the solid product, the aqueous and gaseous phases were not studied further.

2.3. Characterization of the solid products

2.3.1. Higher heating value (HHV)

The ASTM D240 procedure was used to calculate the HHV of the sample utilizing an IKA C 200 bomb calorimeter (Stauffen, Baden-Württemberg, Germany). Before doing the analysis, 0.5 g of the sample was dried at 105 °C for 12 h. In order to determine the ash content of the solid sample, the ASTM D 1102 method was used. The experimental procedure involved heating a dry sample weighing between 0.5 and 2.0 g in a muffle furnace at a temperature of 575 °C for a duration of 6 h. To ensure accuracy, each experiment was repeated three times. The resulting ash from each experiment was collected and stored in a ziplock bag for subsequent analysis using Energy dispersive X-ray (EDX). The HHV results were presented on a dry free basis. The following equation was utilized to determine the energy yield, EY (%):

$$EY\,(\%) = SY\,(wt\%) \times \frac{\text{HHV of dried solid product}}{\text{HHV of dried Feedstock}} \quad (2)$$

2.3.2. Ultimate analysis

Quantification of nitrogen, hydrogen, carbon, and sulfur content of co-HTT_SP was accomplished using a CHNS analyzer (Thermo FLASH EA 1112 Series). The analysis was conducted in accordance with ASTM D5373. Vanadium pentaoxide was utilized as a conditioner, and 2, 5-Bis (5-*tert*-butyl-benzoxazol-2-yl) thiophene was utilized as a calibration standard (Ghalandari et al., 2022a). Each sample was burned at 950 °C in oxygen (the carrier gas was helium). A difference approach was used to obtain the oxygen concentration. It should be noted that nitrogen, hydrogen, carbon, and sulfur content of AHC was obtained in the previous study (Volpe et al. 2021).

2.3.3. Proximate analysis

Fixed carbon (FC) and the volatile matter (VM) of the solid samples were determined by Perkin Elmer's TGA 4000 thermogravimetric analyzer (Waltham, MA, USA). The analysis method was derived from literature (Islam et al. 2021). In order to prevent any kind of oxidation process and purge the VM at the same time, the analysis was conducted with a constant flow of nitrogen gas (40 mL/min). The sample was initially heated to 110 °C at a rate of 20 °C/min, and then it was maintained in an isothermal condition for 5 min. In the second step, the sample was heated at a rate of 20 °C/min to 900 °C, and then it was maintained in an isothermal environment for 10 min. The VM was determined based on the amount of mass lost between 110 and 900 °C. In the end, a difference of VM and ash was used to calculate the FC.

2.3.4. Energy dispersive X-ray

The semi-quantitative inorganic analysis of ash samples was determined with the use of an energy dispersive X-ray (EDX) analyzer (Octane plus, EDAX, USA). All samples were given a coating of gold using vacuum sputtering equipment called a Denton Vacuum Desk III (Moorestown, NJ, USA). Slagging, fouling, alkali, and ratio-slag indexes, and Cl content were calculated based on Table 1 (Tortosa Masiá et al. 2007). The correlations have the form B/A, where B represents compounds with a low melting point ($CaO + Cr_2O_3 + Fe_2O_3 + Mo_2O_3 + WO_2$) and A represents compounds with a higher melting point ($SiO_2 + TiO_2 + Ni_3O_4 + Al_2O_3$).

2.3.5. XRD analysis of WPVC and co-HTT_SP

The X-ray powder diffraction technique was used to examine the level of crystallinity in the samples of WPVC and co-HTT_SP ash. This analysis was carried out using a Bruker AXS X-ray diffraction system (D2 Phaser SSD160) made in Karlsruhe, Germany. The X-ray emission parameters were configured with an operating voltage of 30 kV and a current of 10 mA. A copper tube with a wavelength of 1.54184 Ã… was employed. Data collection was performed within an angular range of 5 to 80° (2θ) under normal atmospheric pressure.

Table 1
Slagging, fouling, alkali, and ratio-slag indexes, and Cl content, definition and their limits (Reza et al. 2013).

Index	Expression	Limit
Slagging index	$I_S = (B/A) \times S^d$ S^d = % of S in dry fuel	$I_S < 0.6$ (I_S is low slagging inclination)$I_S = 0.6$—2.0 (I_S is medium)$I_S = 2.0$—2.6 (I_S is high)$I_S > 2.6$ (I_S is extremely high)
Fouling index	$I_F = (B/A) \times (Na_2O + K_2O)$	$I_F \leq 0.6$ (I_F is low fouling inclination) $0.6 < I_F < 40$ (I_F is medium)$I_F \geq 40$ (I_F is high)
Alkali index	$I_A = (Na_2O + K_2O)$ in kg/GJ	$0.17 < I_A < 0.34$ (I_A is slagging/fouling probable$I_A \geq 0.34$ (I_A is slagging/fouling is certain)
Slag viscosity index	$I_V = (SiO_2 \times 100)/(SiO_2 + MgO + CaO + Fe_2O_3)$	$I_V > 72$ (I_V is low slagging inclination65 $\leq I_V \leq 72$ (I_V is moderate)$I_V < 65$ (I_V is high)
Chlorine content	Cl (wt%)	Cl < 0.2—0.3 (Cl is low slagging inclination)0.2 < Cl < 0.3 (Cl is medium)0.3 < Cl < 0.5 (Cl is high)Cl > 0.5 (Cl is extremely high)

2.3.6. Fourier-transform infrared spectroscopy

Thermo Scientific's attenuated total reflector (Nicolet iS5) was utilized to identify the functional groups present in the solid samples (Madison, WI, USA). Resolution was set to 4 cm^{-1}, data accumulation was set to 64, and the wavenumber range was set to 400–4000 cm^{-1} (Banivaheb et al. 2022).

2.3.7. Chlorine content measurement

A Dionex Aquion IC (ion chromatography) system (Thermo Scientific) was utilized to determine the chlorine content in the (dissolved) solid product and the aqueous phase. The digestion method (Pettersson and Olsson 1998) was used to prepare the liquid sample from the solid product to inject into IC. Nitric acid (2 mL) and solid product (10 mg) was first added to a chemical volumetric flask for digestion. The mixture was heated on the electrical heater for 60 min at 80 °C. After that, it was let to reach ambient temperature. The mass loss that occurred in this digestion process was noted. 2 mL of hydrogen peroxide was added in the next step. After an additional 60 min of the heating mixture at 80 °C, it was let to cool down to room temperature. After that, the mixture was diluted with DI water to prepare the sample to inject into IC in order to determine the chlorine content in the solid product. To determine the chlorine content in the aqueous phase, the aqueous phase was diluted with DI water for injection in IC. For the purpose of calculating DE, the following equation was utilized:

$$DE\,(\%) = \frac{C_1 - C_2}{C_1} \times 100 \quad (3)$$

where C_1 and C_2 indicate the chlorine mass of the feedstock and solid product (in a dry mass basis), respectively.

2.3.8. Combustion test

Perkin Elmer's TGA 4000 thermogravimetric analyzer (Waltham, MA, USA) was used to conduct the combustion test. A crucible was filled with 5–10 mg of the sample, while a 40 mL/min of air flow was continuously blown through it. The temperature rose from 30 to 900 °C in three stages: steady at 35 °C for 10 min, rising to 110 °C and maintaining it for 5 min, and finally increasing to 900 °C at a rate of 20 °C/min. The initial weight loss temperature, denoted by T_i, the burnout temperature, denoted by T_f, the maximum burning rate, denoted by DTG_{max}, and the average burning rate, denoted by DTG_{mean}, are the characteristic parameters of the combustion test. The comprehensive combustion index, denoted by the letter S, was calculated using following equation (D. Zhao et al. 2016; G. Wang et al. 2015; 2016):

$$S = \frac{DTG_{max} \times DTG_{mean}}{T_i^2 \times T_f} \quad (4)$$

3. Results and discussions

3.1. Role of AHC on dechlorination of WPVC

The chlorine content in the solid phase and aqueous phase as well as the pH of the aqueous phase are presented in Table S1. Based on the results, the chlorine content of WPVC reduces significantly after co-HTT. According the literature, most of chlorine of PVC goes to aqueous phase from solid phase through HTT, and chlorine does not go to the gas phase (Poerschmann et al. 2015; Takeshita et al. 2004). As shown in Table S1, a small fraction of chlorine is lost during sample collection in addition to measurement errors (P. Zhao et al. 2017). It can be seen in Table S1, the chlorine content of WPVC decreases from 552.5 (g/kg) to 3.0 (g/kg) for solid product at 350 ℃, 1 h (in presence of 5% AHC). It should be noted

that adding AHC has a dilution effect for chlorine content of solid samples since the AHC has no chlorine content. The pH of aqueous phase is low (between 1.34 and 2.01) thus giving substantial indication that the main mechanism pathway was the dehydrodechlorination followed by dehydration with the release of HCl.

The DE of WPVC is shown in Fig. 1a. The findings demonstrate that AHC loading has a substantial influence on DE. This behavior is consistent with previously published investigations on HTT dechlorination (Shen 2016). Fig. 1a shows that adding AHC from 0 to 5 wt% (at 0.5 h and 325 °C) dramatically enhances the DE from 89.35 to 97.66%. It might be the result of synergy between the complex lignocellulosic components and chlorinated feedstock (Y. Zhao et al. 2022). After that, increasing AHC loading ratio from 5 to 20 wt% has no influence on WPVC dechlorination in the co-HTT. This finding suggests that the ideal AHC loading ratio is 5 wt%.

Fig. 1a also illustrates that the co-HTT temperature has a substantial impact on chlorine removal, as the DE rises dramatically from 89.38% at 300 °C to 98.67% at 350 °C (at 0.5 h and in the presence of 5 wt% of AHC). It demonstrates that the co-HTT removes the majority of chlorine from WPVC; nevertheless, a small quantity of chlorine still remained in the solid product. These organic chlorine atoms that are still present may be carbon atoms with sp^2-hybridized in olefinic and aromatic structures that are resistant to the nucleophilic substitution process that is carried out by hydroxyl ions (Poerschmann et al. 2015). While DE of PVC pyrolysis at 300 °C for 3 h was measured to be 90% (Ma et al., 2002), the DE for co-HTT of PVC at the same temperature but with a significantly shorter residence time of 1 h is also approximately 90% (Fig. 1a). This highlights the notable benefit of co-HTT, as it achieves comparable DE to pyrolysis while requiring a substantially shorter residence time. As can be seen in Fig. 1a, by adding 5 wt% AHC at the same temperature (325 °C) the DE increases from 89.35 to 97.66%, and by increasing temperature from 300 to 350 °C (at 0.5 h) in the presence of 5 wt% AHC, the DE increases from 89.38 to 98.67%. Also, the residence time could play a role, in fact, the highest DE (99.46%) was achieved at 5% of AHC loading, 350 °C, and 1 h residence time.

As demonstrated in Fig. 1a, by raising the reaction time from 0.25 to 1 h at 350 °C, the DE increases from 93.58 to 99.46%, which however declines to 97.26% after 4 h. This finding is consistent with earlier HTT dechlorination research that has been reported in the literature (Y. Zhao et al. 2022; Li et al. 2017). This may be attributed to the carbonization and formation of pores at longer reaction time, which increases the adsorption capacity of co-HTT_SP. Hence, a portion of dissolved chlorine in the water might be adsorbed onto the solid product, resulting in a decrease in DE (Y. Zhao et al. 2022).

The removal of chlorine from WPVC might be accomplished via elimination and substitution reactions. The elimination process begins with the creation of thermally unstable free radicals and chloroallylic compounds, followed by the removal of HCl to produce polyenes (Shen 2016). After that, the allyl chlorine atom on the C–atom would separate into —Cl and —H to generate two double bonds. In this manner, the zipper mechanism completes the dehydrochlorination process by activating successive chlorine molecules (Poerschmann et al. 2015; D. Ma et al. 2019), which is corroborated by the 1620 cm^{-1} transmittance band showed in Fig. 1b. This peak becomes evident after co-HTT, coinciding with an increase in the strength of C═C stretching vibrations. There are typically two ways that the substitution occurs. The first, which is supported by FTIR results (Fig. 1b), is that —H and —Cl are substituted with two —OH on a carbon to produce unstable intermediates, which is then followed by a dehydration process to produce —C═O and H_2O (P. Zhao et al. 2017). The peaks detected at around 1740 cm^{-1} are ascribed to the C═O stretching vibration, which is clearly enhanced in co-HTT_SP. Furthermore, two other peaks change are occurring into the co-HTT_SP: the drop in the aliphatic C—Cl stretching vibration peak at around 717 cm^{-1} indicates that a portion of chlorine is removed; in contrast, the bands at 1015 cm^{-1}, due to the vibration of C—OH groups connected to alkyl groups, become more prevalent. The difference between these two peaks might indicate that the —Cl is immediately substituted with —OH through the second above mentioned pathway. In polymers, hydroxyl groups take the place of chlorine atoms to yield intermediates such as polyols, diols, and alcohols that might undergo reactions to form aromatic compounds and low molecular weight molecules with O—functionalization (Poerschmann et al. 2015; Huang et al. 2019). As indicated before, the removal of HCl and the replacement of —Cl might form soluble inorganic chlorine, resulting in the elimination of chlorine from WPVC. There are two ways in which the breakdown of lignocellulosic components might accelerate the dechlorination process. First, the breakdown of cellulose, hemicellulose, and lignin might supply an abundance of free —OH bonds (Tekin, Karagöz, and Bektaş 2014), hence facilitating the replacement of —Cl in chlorinated polymers (Yao and Ma 2018). Second, the tiny free cellulosic pieces in the solution may inhibit the agglomeration of plastics and promote the homogeneity of mixes by adhering to the surface of molten polymers (D. Ma et al. 2019). High co-HTT process temperature could, in contrast, produce considerable amounts of oxygenated compounds like furans and furfurals which could eventually undergo condensation onto unreacted PVC decreasing DE (Yao and Ma 2018). In the case of AHC, produced at 250 °C, the hemicellulose and cellulose fraction are virtually absent thus drastically reducing the production of condensing species while still providing free OH groups by decomposition non soluble lignin fraction into polyphenols (Volpe et al. 2020). Thus, the WPVC DE might be governed by the amount of free OH groups produced by HTT decomposition but limited by the formation of oxygenated organic species that condensing could increase WPVC agglomeration thus decreasing its wettability and reactivity. WPVC morphology and porosity drastically influence its wettability and thus influence the DE (D. Ma et al. 2021). The above mentioned two contrasting effects could explain why the addition of small amounts of AHC could promote DE but increased amounts of AHC could lead to WPVC agglomeration phenomena depressing the efficiency of reaction. A proposed reaction mechanism of co-HTT of WPVC is presented in Fig. 1c based on above explanation. It appears that the reusability of AHC is not possible because one portion of it degrades during the co-HTT process. The remaining part, which is mixed with WPVC char, might have different properties compared to raw AHC.

3.2. Physicochemical properties of Co-HTT solid residues

To assess the influence of AHC on the co-HTT of WPVC, AHC loadings ranging from 0 to 20 wt% (at 325 °C and 0.5 h) were used in co-HTT experiments. The solid yield under a variety of co-HTT conditions is shown in Table 2. In the first, HTT experiment as a control run, WPVC (AHC loading = 0 wt%) was loaded and the reaction temperature and time were 325 °C and 0.5 h, respectively. It can be seen in Table 2, SY for the control run is 71.47 wt%. When 5 wt% of AHC was added during co-HTT at 325 °C and 0.5 h SY drastically reduced from 71.47 to 49.75 wt %. A recent study revealed that loading coal can improve the solid yield in the co-hydrothermal process of WPVC (P. Zhao et al. 2020). The synergistic interaction of complex components of WPVC and AHC may expedite the breakdown of feedstock, which may be one of the primary causes of the decrease in solid output (Y. Zhao et al. 2022). Zhang et al. (Zhang, Zhang, and Li 2019) reported that the synergistic interaction might accelerate the decomposition of PVC and pinewood.

To determine the impact of reaction temperature on SY, a number of high temperature co-HTT experiments were carried out at 0.5 h with a 5 wt% AHC loading. Table 2 demonstrates that the co-HTT temperature has a substantial influence on SY, as the yield declines from 59.75 wt% at 300 °C to 44.17 wt% at 350 °C. Zhao et al. (P. Zhao et al. 2020) also showed that a rise in temperature can reduce the solid yield during the co-hydrothermal carbonization of coal and PVC. The findings indicate that the kinetics of the reaction at 300 °C is sluggish, and this temperature is inadequate to break the polymer chains of PVC into shorter lengths. However, high temperature co-HTT could overcome this

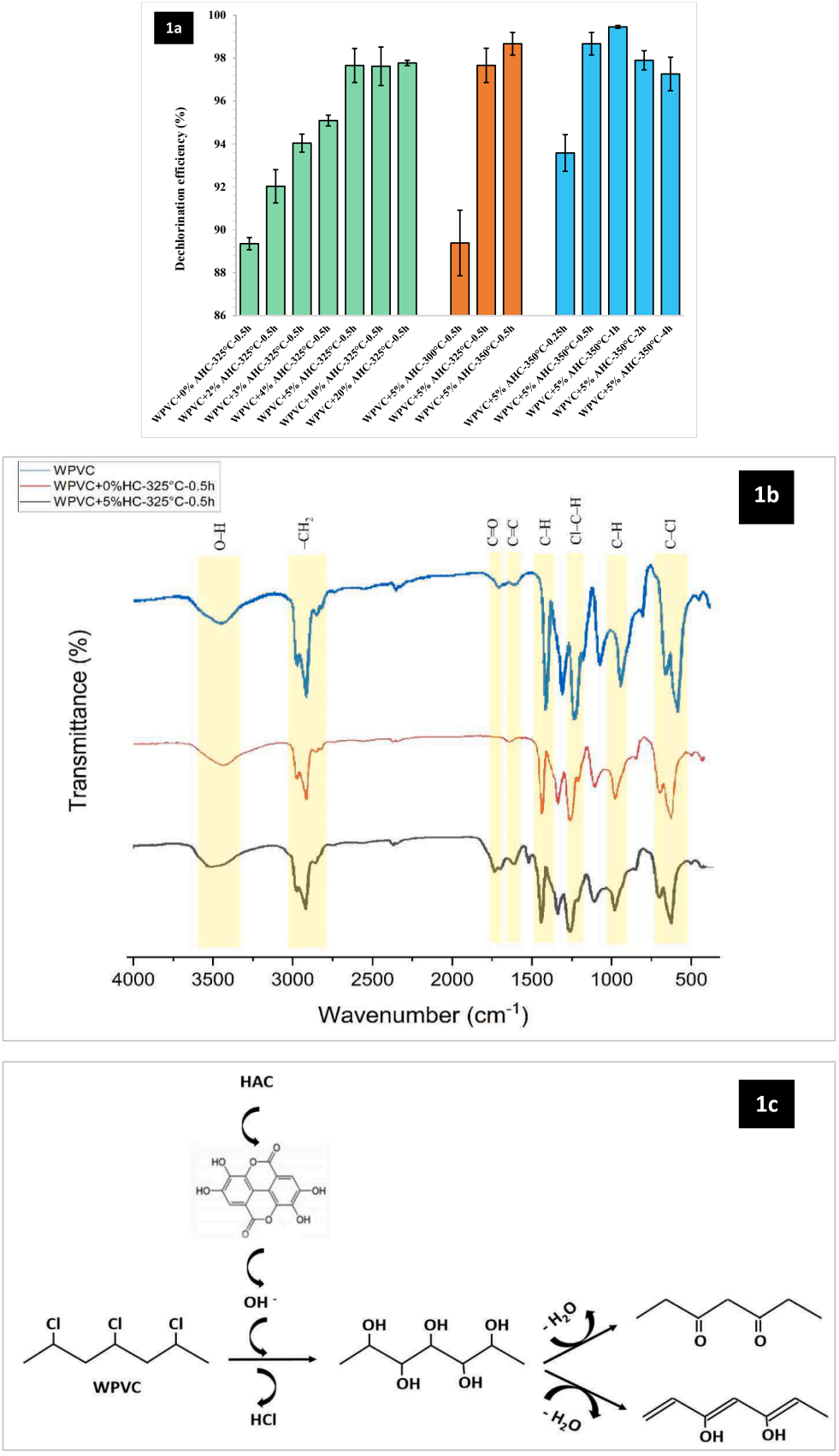

Fig. 1. (1a) The DE of WPVC after co-HTT at different conditions; (1b) FTIR analysis of the WPVC, and co-HTT_SP in presence of AHC at 325 °C, 0.5 h and in absence of AHC at 325 °C, 0.5 h; (1c) the proposed reaction mechanism of co-HTT of WPVC (adapted from Ma. et al. 2021 (D. Ma et al. 2021)).

Table 2
Solid yield, proximate and ultimate analysis of AHC, WPVC, and co-HTT_SP at different process conditions.

Sample	Solid yield (wt %)	Proximate analysis[a]			Ultimate analysis[a]				
		VM (wt%)	FC[b] (wt %)	Ash (wt%)	C (wt%)	H (wt%)	S (wt%)	O[c] (wt%)	Cl (wt%)
AHC	–	56.28 ± 2.56	43.19	0.53 ± 0.13	65.47 ± 4.25	4.78 ± 0.88	BD	29.22	BD
WPVC	–	84.10 ± 1.48	10.25	5.65 ± 0.24	34.69 ± 1.34	4.18 ± 1.65	0.42 ± 0.03	–	55.25 ± 3.35
AHC-325 °C-0.5 h	70.25 ± 1.56	40.25 ± 1.85	59.00	0.75 ± 0.11	75.35 ± 3.21	6.23 ± 0.35	BD	18.42	0.0
WPVC + 0% AHC-325 °C −0.5 h	71.47 ± 1.72	55.98 ± 2.35	35.12	8.90 ± 0.99	62.85 ± 3.98	5.94 ± 0.52	0.21 ± 0.05	7.20	14.9 ± 0.5
WPVC + 2% AHC-325 °C-0.5 h	64.67 ± 3.87	49.64 ± 1.52	42.11	8.25 ± 2.45	67.21 ± 2.52	5.78 ± 0.35	0.15 ± 0.05	6.28	12.33 ± 1.5
WPVC + 3% AHC-325 °C-0.5 h	58.21 ± 4.59	49.12 ± 1.65	42.55	8.33 ± 1.28	68.46 ± 4.25	6.38 ± 1.20	0.25 ± 0.08	6.34	10.24 ± 0.9
WPVC + 4% AHC-325 °C-0.5 h	52.51 ± 2.83	46.10 ± 2.22	45.89	8.01 ± 1.79	70.23 ± 0.89	5.92 ± 0.75	0.31 ± 0.02	6.18	9.35 ± 0.6
WPVC + 5% AHC-325 °C-0.5 h	49.75 ± 4.9	44.90 ± 3.52	47.50	6.60 ± 3.25	74.29 ± 1.42	6.21 ± 1.12	0.22 ± 0.04	7.97	4.71 ± 0.2
WPVC + 10% AHC-325 °C-0.5 h	50.95 ± 1.05	43.70 ± 0.89	50.09	5.21 ± 0.95	74.56 ± 2.25	5.97 ± 0.35	0.11 ± 0.02	8.48	5.67 ± 1.2
WPVC + 20% AHC-325 °C-0.5 h	51.49 ± 2.70	42.28 ± 3.23	52.06	4.66 ± 1.02	75.28 ± 1.88	5.26 ± 0.54	0.15 ± 0.03	8.64	6.01 ± 0.3
WPVC + 5% AHC-300 °C-0.5 h	59.75 ± 2.97	60.70 ± 1.78	33.13	6.17 ± 0.56	62.61 ± 2.52	5.08 ± 1.85	0.08 ± 0.02	8.29	17.77 ± 3.2
WPVC + 5% AHC-350 °C-0.5 h	44.17 ± 1.40	45.80 ± 1.95	45.09	9.11 ± 1.52	77.07 ± 1.35	7.11 ± 1.52	0.26 ± 0.01	5.44	1.01 ± 0.5
WPVC + 5% AHC-350 °C-0.25 h	59.35 ± 4.34	57.20 ± 0.35	35.75	7.05 ± 4.21	70.82 ± 0.95	6.71 ± 0.22	0.21 ± 0.01	4.39	10.82 ± 2.1
WPVC + 5% AHC-350 °C-1 h	42.72 ± 1.29	44.30 ± 2.65	46.38	7.32 ± 2.38	78.89 ± 3.32	7.25 ± 0.12	0.09 ± 0.01	3.18	3.27 ± 0.25
WPVC + 5% AHC-350 °C-2 h	46.40 ± 1.60	42.20 ± 1.25	49.77	6.03 ± 0.87	79.93 ± 2.85	7.26 ± 0.05	0.16 ± 0.04	3.15	4.53 ± 0.76
WPVC + 5% AHC-350 °C-4 h	48.80 ± 7.21	42.30 ± 1.30	49.27	6.13 ± 0.55	80.02 ± 1.95	7.15 ± 1.23	0.14 ± 0.02	2.95	4.61 ± 0.98

[d]BD: Below detection limit.
[a] Dry basis.
[b] FC (wt%) = 100 – VM (wt%) – Ash (wt%).
[c] O (wt%) = 100 – C (wt%) – H (wt%) – N (wt%) – S (wt%) – Cl (wt%).

sluggish kinetics. Moreover, large intermediate monomers are formed during condensation, cyclization, and cross-linking processes as the co-HTT temperature continues to rise. At the same time, aromatization and polymerization occur, which resulted in the formation of a condensed carbon network (B. Patel et al. 2016). By prolonging the reaction time from 0.25 to 1 h, SY reduces from 59.35 to 42.72 wt%, as shown in Table 2; nevertheless, it decreases further after 1 h. Similar finding were observed by Zou et al. (Zou et al. 2009) for the variation of SY with reaction time. The reason might be due to the competition between hydrolysis and repolymerization. The feedstock is initially broken down and turned into monomers, and when the reaction time is prolonged, these monomers may subsequently rearrange to generate solid residues via condensation, cyclization, and polymerization (Zou et al. 2009).

Proximate and ultimate analyses were conducted on the solid samples to determine the change in fixed carbon/volatile content and elemental composition, respectively, and the results have been presented in Table 2. By comparing the VM of feedstock and co-HTT_SP, it is clear that co-HTT decreases the VM significantly. The VM of the co-HTT_SP decrease from 55.98 to 49.64 wt% by loading only 2 wt% of AHC. The VM further decreases from 49.64 to 42.28 wt% by loading additional AHC. When the co-HTT temperature is raised from 300 to 350 °C, the VM of co-HTT_SP reduces from 60.7 to 45.8 wt%, and it reduces from 57.2 to 42.3 wt% when the reaction time is increased from 0.25 to 4 h. Zhao et al. showed when the temperature increases, the VM content of WPVC decreases (Zou et al. 2009). By comparing the FC of feedstock co-HTT_SP, it can conclude that the co-HTT leads to an opposite trend of FC compared to VM as the FC of co-HTT_SP increases up to 52.19 wt% when 20 wt% AHC was added at 325 °C and 0.5 h. Yao and Ma also demonstrated that the FC of co-HTT_SP increases by loading biomass (bamboo) and increasing temperature during co-HTT of WPVC (Yao and Ma 2018).

The ultimate analysis that co-HTT_SP have a greater concentration of carbon and hydrogen in comparison to WPVC. When AHC loading increases from 0 to 20 wt%, the concentration of solid products rises from 62.85 to 75.28 wt% and the oxygen concentration increased from 7.20 to 8.64 wt%. The increase in co-HTT temperature (from 300 to 350 °C) results in a considerable (14.46 wt%) increase in carbon content, and decrease of oxygen content by about 2.85 wt% (Garlapalli et al., 2016). Moreover, hydrogen content of co-HTT_SP ranging from 5.08 to 7.26 wt %. It should be noted that the sulfur contents remained negligible, and the nitrogen content was below detection limit of the CHNS analyzer (0.5 wt%). Literature reported similar findings for sulfur, hydrogen, and nitrogen contents (Yao and Ma 2018). According to the Van Krevelen diagram (Fig. 2a), loading AHC causes a reduction in the H/C atomic ratio. The addition of AHC (adding more carbon without significant hydrogen addition) and the decomposition of PVC (releasing hydrogen-rich species) causes a reduction in the H/C atomic ratio. An increase in temperature causes a decrease in the O/C atomic ratio and an increase in the H/C atomic ratio. Increasing the temperature during HTT of PVC causes a decrease in the O/C atomic ratio due to the release of oxygen-containing compounds and the production of additional carbonaceous material. Simultaneously, the H/C atomic ratio increases because the thermal decomposition of PVC generates hydrogen-rich species, increasing the hydrogen content in the system. Furthermore, increasing the reaction time decreases the O/C and H/C atomic ratios. The reason might be due to the generation of carbonaceous material and the

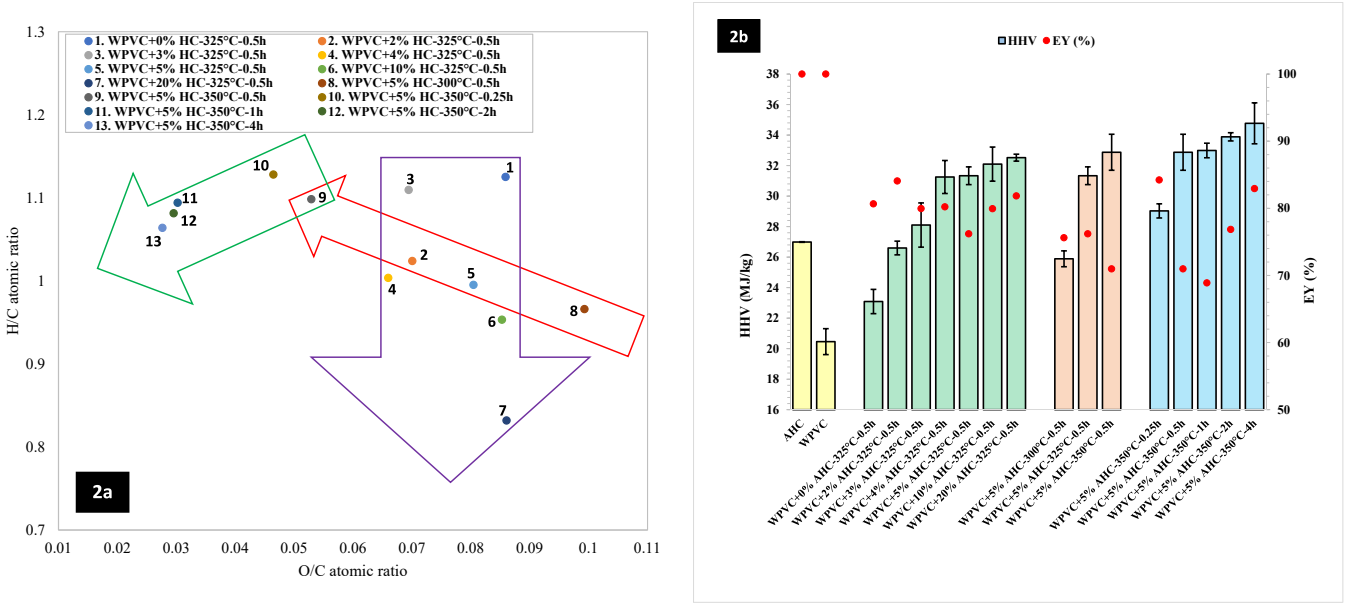

Fig. 2. (2a) Van Krevelen diagram of co-HTT_SP produced at various co-HTT conditions (purple arrow: effect of increasing AHC loading ratio, green arrow: effect of increasing reaction time, red arrow: effect of increasing reaction temperature); (2b) Higher heating value (HHV) and energy yield (EY) of AHC, WPVC, and co-HTT_SP produced at various co-HTT conditions. (For interpretation of the references to colour in this figure legend, the reader is referred to the web version of this article.)

removal of oxygen-containing compounds. Increasing the reaction time alone does not inherently decrease the H/C atomic ratio. It is possible that other factors or reactions occurring during the extended reaction time may influence the H/C atomic ratio, but it cannot be generalized as a direct relationship.

XRD analysis of WPVC ash and co-HTT_SP ashes were carried out to investigate the crystallinity of the samples. WPVC ash XRD spectrum (Fig. S1) shows a high amorphous degree when compared to the to the crystallinity of the ash of co-HTT_SP obtained 325 °C,0.5 h, 0 wt% AHC (Fig. S2) and the ash sample of co-HTT_SP 325 °C,0.5 h, 5 wt% AHC (Fig. S3). Both these two samples show very similar composition with crystal compounds mainly resembly those of Orthopyroxenes, Polyhalites and Clinozoisites.

3.3. Fuel and combustion properties of co-HTT solids

Fig. 2b shows that the HHV of solid products increases significantly from 23.06 to 32.52 MJ/kg by increasing AHC loading from 0 to 20 wt%. However, EY fluctuated from 80.66 to 75.61% by adding AHC. As a result of the increase in co-HTT temperature from 300 to 325 °C, the HHV increases significantly from 25.89 to 31.33 MJ/kg, and it increases slightly from 31.33 to 32.87 MJ/kg by raising the temperature from 325 to 350 °C. The impact of temperature on EY is completely different from the impact of it on HHV. The results show that EY decreases from 75.61 to 70.97% when the temperature rises from 300 to 350 °C. The reaction time has a constructive influence on the HHV since it increases from 29.03 to 34.77 MJ/kg by raising it from 0.25 to 4 h. The co-HTT of WPVC increases the carbon and hydrogen content mostly owing to the dehydrochlorination process (Yao and Ma 2018). Because of the high carbon and hydrogen content, the solid product obtained from WPVC (in the presence of 5 wt% AHC) has an HHV of about 34.77 MJ/kg at 350 °C and 4 h. Although the EY reduces from 84.21 to 68.88% by raising the reaction time from 0.25 to 1 h, it rises from 68.88% to 82.93% when the reaction time is raised from 1 to 4 h.

TGA was used to evaluate the combustion properties of raw materials (WPVC and AHC). Fig. 3a displays the TG and DTG curves for AHC. Based on the DTG curve, the combustion occurs at 317–656 °C due to the low quantity of volatile chemicals in AHC. The DTG curve of WPVC combustion could be separated into two sections. The initial peak is strong (between 276 and 398 °C) corresponding to the dehydrochlorination process, with a weight loss of 55.6%. The second peak is weak (between 442 and 518 °C), with a weight loss of 16.1 wt%, and is associated with the burning of volatiles and fixed carbon.

The combustion properties of co-HTT_SP were evaluated, and Fig. 3 (a-c) depicts their TG and DTG curves. Inferred from the TG curves, the burning process consists of one step, which is less than that of WPVC, indicating that co-HTT enhanced the feedstock's homogeneity. This is because of the less amount of CH—Cl bonds in the solid products; hence, the combustion of the dehydrochlorination process is not significant to show a peak. The only exception is for the co-HTT solid with 20 wt% AHC (at 325 °C and 0.5 h). It can be seen in the DTG curve, there are two peaks for this solid product. The first peak could be related to AHC since the combustion process for it occurs before the WPVC char, and the second peak could be related to the combustion of WPVC char.

In order to determine the effects of different parameters on the combustion behavior of AHC, WPVC, and co-HTT_SP, the TG-DTG method was utilized, and the finding are presented in Table 3. Based on the results, WPVC has a lower T_i when compared to that one of AHC. The reason could be that WPVC contains a large concentration of C—Cl bonds with low bond energy that can be broken at low temperatures (Q. Wang et al. 2018). The co-HTT increased the T_i of WPVC by removing chlorine, forming a carbon chain, and increasing the coalification degree (Lin et al. 2020; Ning et al. 2020). The reaction temperature and time are critical factors in determining the fuel characteristics of solid products. T_i of solid products remains dropping with increasing reaction time and temperature demonstrating the higher reaction temperatures and longer residence times enhance solid residues reactivity. In contrast, the T_f of solid products rises as reaction temperature and time increase, demonstrating that higher temperature or time might push combustion to the high-temperature zone (Lin et al. 2016).

To assess the combustion performance of a solid product as a solid fuel, the comprehensive combustibility index (S) was determined. A high S value correlates with the rate of mass loss and indicates a more intense combustion response. However, a high mass loss rate may result in an unsteady flame and significant heat loss (Jiang et al. 2016). As a consequence of the formation of hydrogen chloride, the high

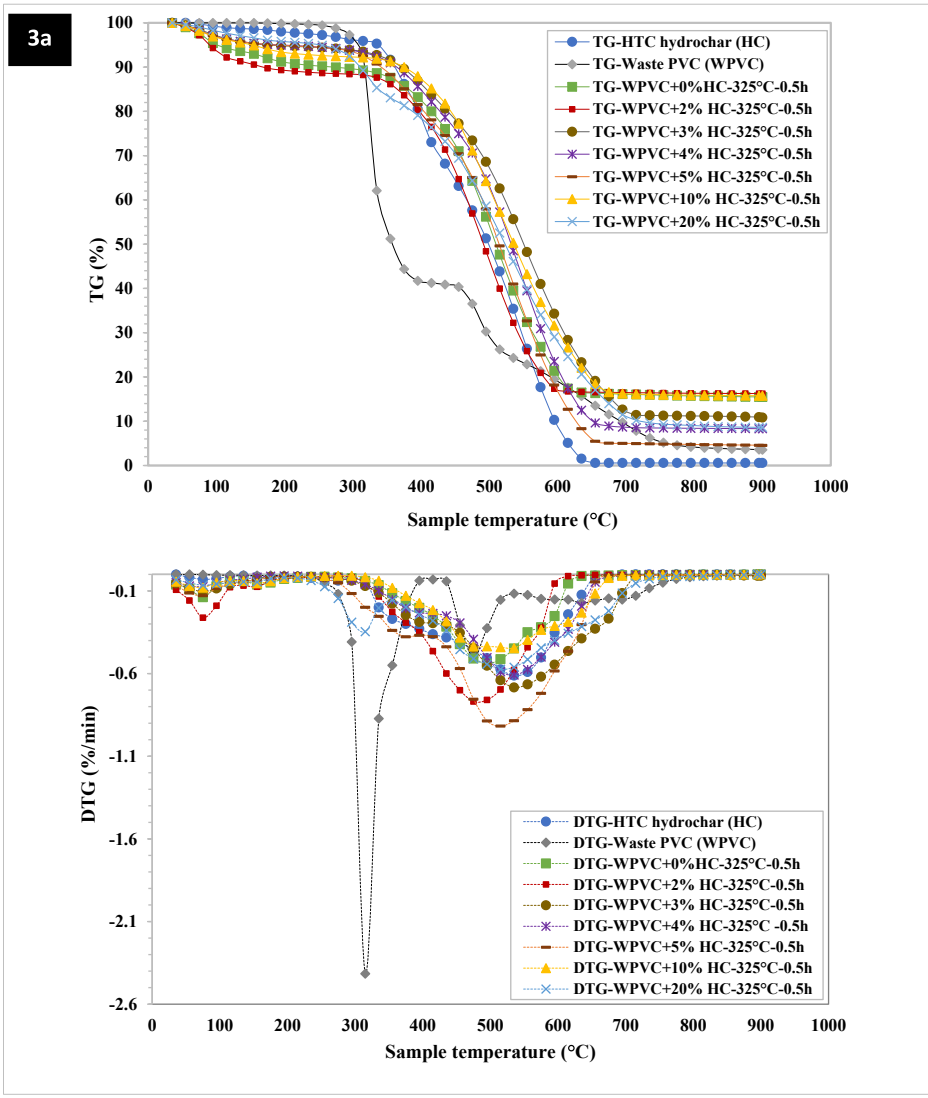

Fig. 3. TG-DTG curves for AHC, WPVC, and co-HTT_SP produced at various co-HTT conditions; (3a) effect of loading AHC; (3b) effect of reaction temperature, (3c) effect of reaction time.

combustibility S index of WPVC may result in an unstable flame. Chlorine content of WPVC decreases during co-HTT; therefore, the detrimental impact of formation of hydrogen chloride on flame would be mitigated (Y. Zhao et al. 2022). Table 3 shows that the combustion performance of co-HTT_SP improves by increasing reaction temperature and time. The S index value of co-HTT_SP increases from 1.06 ($\times 10^{-9}$) to 1.41 ($\times 10^{-9}$) with increasing temperature from 300 to 350 °C, and by increasing reaction residence time from 0.25 h to 4 h, the S index value increases from 0.98 ($\times 10^{-9}$) to 1.82 ($\times 10^{-9}$). This finding may be connected to the development of pores at high temperatures and the combustion-favorable extended reaction time (Y. Zhao et al. 2022). When the S index is greater, the combustion is more intense, and the solid product will burn up more quickly (Lin et al. 2015).

3.4. Slagging and fouling indices of co-HTT solids

Table 4 displays the grades of the fouling index (I_F), slagging index (I_S), slag viscosity index (I_V), alkali index (I_A), and chlorine content for WPVC and co-HTT_SP, based on the EDX analysis result reported in the supplementary material (Table S2). Based on the literature (Tortosa Masiá et al. 2007; Reza et al. 2013; Pronobis 2005), given the composition of ash samples, several correlations are employed to examine the slagging/fouling propensity. It can be seen in Table 4, I_S value of WPVC is extremely high. I_S value is improved during the co-HTT from extremely high to low. The only exception is for solid product at 300 °C and 0.5 h where the I_S value is medium. It shows that the higher co-HTT temperature can improve the I_S value of co-HTT_SP. The I_F and I_A values for WPVC and co-HTT_SP are low due to the absence of alkali elements (K_2O and Na_2O). I_V value of WPVC is high, and the value of this index is high for all co-HTT_SP indicating the co-HTT cannot improve this index. The reason could be the low content of SiO_2 and the high content of CaO in ash. The ash chlorine content decreases after the co-HTT significantly from 10.25 wt% for WPVC to less than 0.05 % for co-HTT_SP. The ash chlorine content for five of the ash samples produced is low, but for the remaining ash samples is medium. Thus, the results show that the co-HTT could make an appropriate solid fuel from WPVC. Furthermore, the I_V value and chlorine content of co-HTT_SP are higher than the hydrochar produced from biomass like switch grass, corn Stover, miscanthus, and rice hull (Reza et al. 2013).

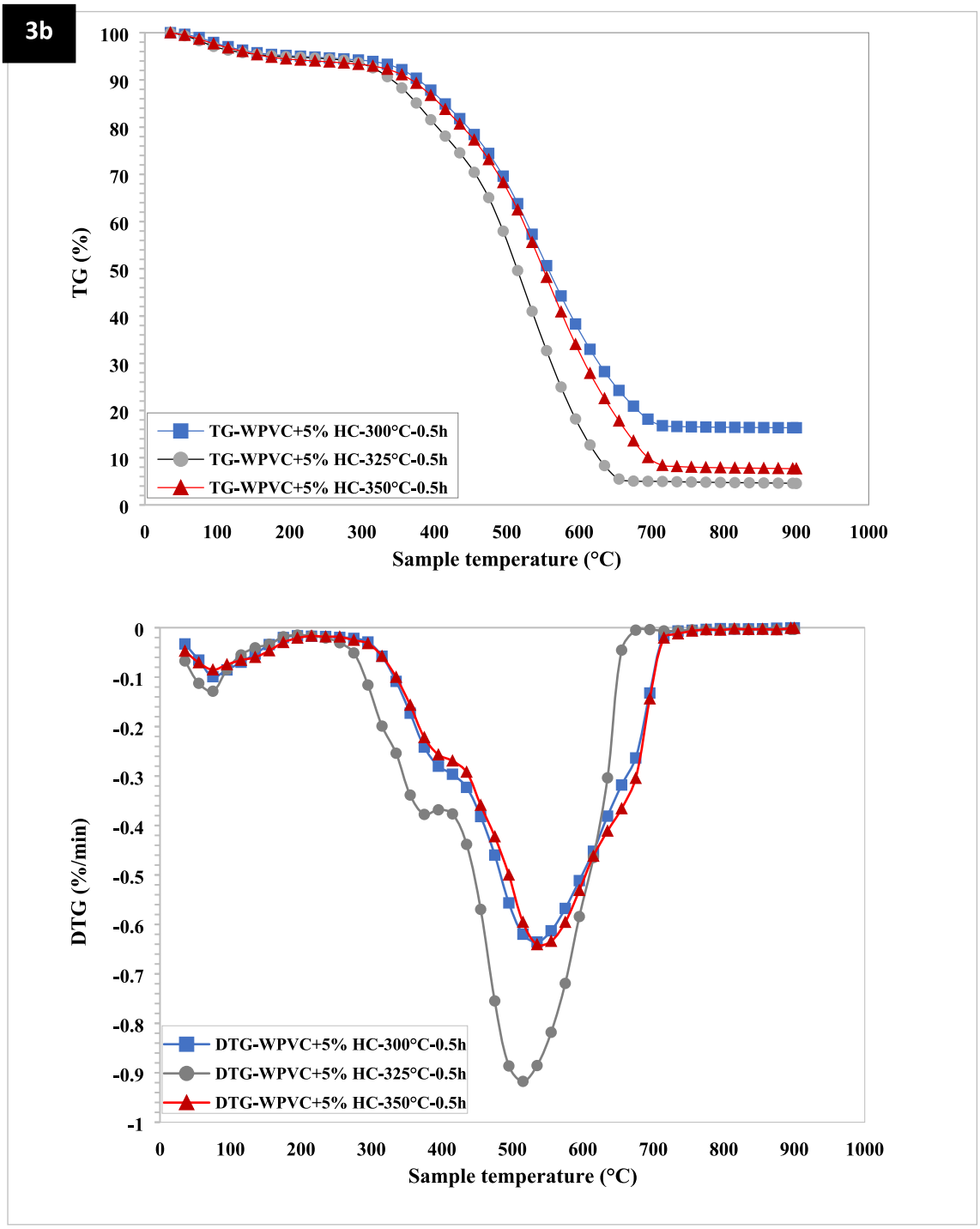

Fig. 3. (*continued*).

4. Conclusions

The present study investigates chlorine migration from the solid residues produced during the co-HTT of waste PVC in the presence of an AHC, and the fuel properties of the co HTT solid products (co-HTT_SP). The results clearly demonstrate that presence of AHC significantly improved the DE. Chlorine migration benefited from the rising co-HTT temperature. DE initially rose as co-HTT duration increases from 0.25 to 1 h, then decreased as co-HTT time increased from 1 to 4 h. At 350 °C, 1 h, in the presence of 5 wt% AHC, gave the highest DE of 99.46%. Moreover, the co-HTT enhanced the HHV of the co-HTT_SP significantly. In terms of combustion, co-HTT_SP demonstrated higher ignition temperature and lower burnout temperature along with a moderate comprehensive combustion index compared to WPVC. Furthermore, the ash of some co-HTT_SP had a low slagging index, fouling index, alkali index, and low/medium chlorine content. These results indicate that the co-HTT considerably enhanced the chlorine removal and combustion properties of WPVC open up the way of an environmentally suitable energy valorization of solid residues obtained via WPVC thermal treatments.

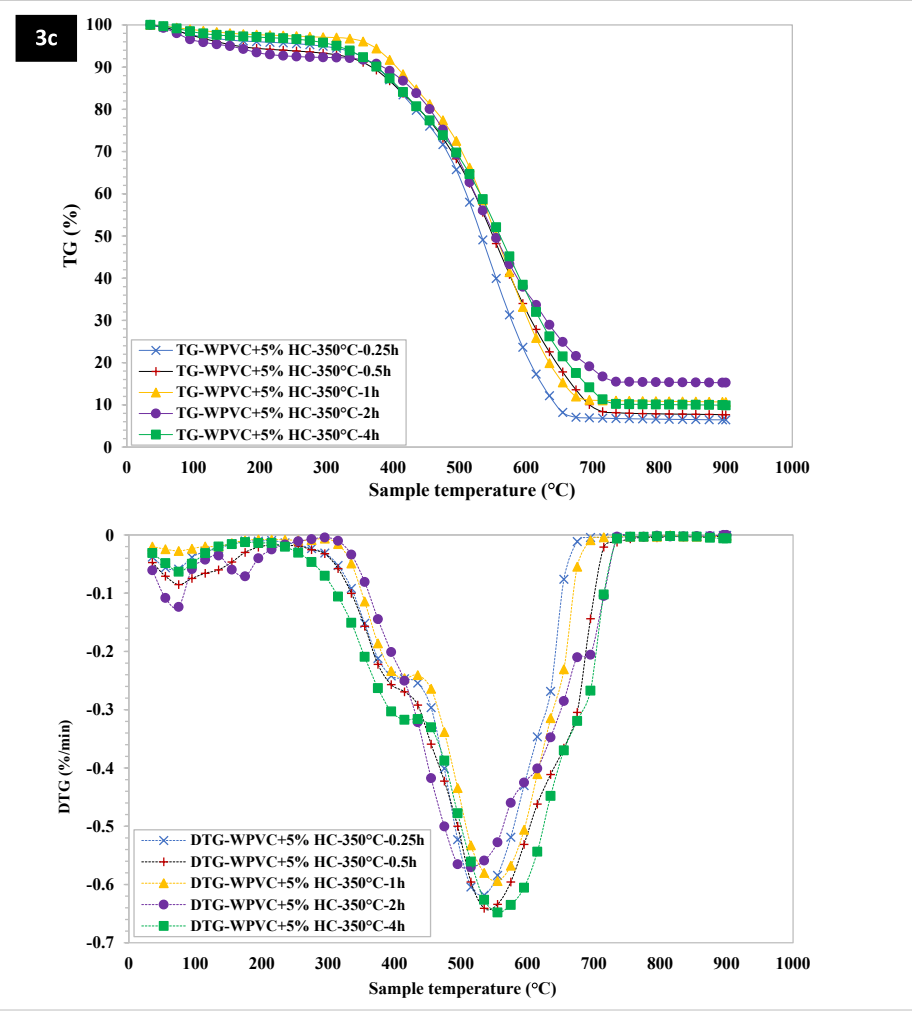

Fig. 3. (*continued*).

Table 3
The combustion characteristic parameters of AHC, WPVC, and co-HTT_SP produced at various co-HTT conditions.

Sample	T_i[a] (°C)	T_f[b] (°C)	T_g[c] (°C)	DTG_{max}(min/%)	DTG_{mean}(%/min)	S (10^{-9}. min^{-2}. C^{-3})
AHC	317.5	555.1	656.5	−0.61	−0.15	1.41
WPVC	276.5	315.1	774.3	−2.42	−0.17	7.06
WPVC + 0% AHC-325 °C-0.5 h	312.4	495.2	637.1	−0.54	−0.11	0.97
WPVC + 2% AHC-325 °C −0.5 h	320.9	475.3	614.9	−0.77	−0.17	2.05
WPVC + 3% AHC-325 °C-0.5 h	322.6	535.4	718.5	−0.68	−0.18	1.68
WPVC + 4% AHC-325 °C-0.5 h	323.5	535.2	666.5	−0.61	−0.14	1.20
WPVC + 5% AHC-325 °C-0.5 h	326.2	515.3	684.4	−0.92	−0.13	1.58
WPVC + 10% AHC-325 °C-0.5 h	334.3	535.2	695.6	−0.45	−0.12	0.68
WPVC + 20% AHC-325 °C-0.5 h	341.1	515.0	730.4	−0.57	−0.18	1.23
WPVC + 5% AHC-300 °C-0.5 h	335.6	555.1	680.1	−0.59	−0.14	1.06
WPVC + 5% AHC-350 °C-0.5 h	316.4	535.8	712.0	−0.64	−0.16	1.41
WPVC + 5% AHC-350 °C-0.25 h	348.2	515.7	677.3	−0.57	−0.14	0.98
WPVC + 5% AHC-350 °C-1 h	324.2	535.8	711.9	−0.62	−0.17	1.37
WPVC + 5% AHC-350 °C-2 h	317.2	535.3	715.1	−0.64	−0.18	1.58
WPVC + 5% AHC-350 °C-4 h	303.0	555.2	732.7	−0.65	−0.19	1.82

[a] T_i, the ignition temperature.
[b] T_f, the burnout temperature.
[c] T_g, the temperature according to DTG_{max}.

Funding

The material is based upon work partially supported by National Science Foundation under Grant No. 2123495.

Data Availability Statement: Not applicable.

CRediT authorship contribution statement

Vahab Ghalandari: Writing – original draft, Formal analysis, Data curation, Conceptualization, Writing – review & editing. **Maurizio Volpe:** Formal analysis, Data curation, Conceptualization, Writing –

Table 4
Slagging, fouling, alkali, and ratio-slag indices, and Cl content of co-HTT_SP ash.

Sample	I_S	I_F	I_A	I_V	Cl
WPVC	Extremely high	Low	Low	High	Medium
WPVC + 0% AHC-325 °C-0.5 h	Low	Low	Low	High	Medium
WPVC + 2% AHC-325 °C-0.5 h	Low	Low	Low	High	Medium
WPVC + 3% AHC-325 °C-0.5 h	Low	Low	Low	High	Medium
WPVC + 4% AHC-325 °C-0.5 h	Low	Low	Low	High	Medium
WPVC + 5% AHC-325 °C-0.5 h	Low	Low	Low	High	Low
WPVC + 10% AHC-325 °C-0.5 h	Low	Low	Low	High	Medium
WPVC + 20% AHC-325 °C-0.5 h	Low	Low	Low	High	Medium
WPVC + 5% AHC-300 °C-0.5 h	Medium	Low	Low	High	Medium
WPVC + 5% AHC-350 °C-0.5 h	Low	Low	Low	High	Low
WPVC + 5% AHC-350 °C-0.25 h	Low	Low	Low	High	Medium
WPVC + 5% AHC-350 °C-1 h	Low	Low	Low	High	Low
WPVC + 5% AHC-350 °C-2 h	Low	Low	Low	High	Low
WPVC + 5% AHC-350 °C-4 h	Low	Low	Low	High	Low

review & editing. **Fabio Codignole Lùz:** Formal analysis, Data curation, Conceptualization, Writing – review & editing. **Antonio Messineo:** Formal analysis, Data curation, Conceptualization, Writing – review & editing. **Toufiq Reza:** Funding acquisition, Conceptualization, Project administration. Author Dr. Tousif Reza has acquired funding from NSF, rest authors contributed to the review and editing.

Declaration of Competing Interest

The authors declare that they have no known competing financial interests or personal relationships that could have appeared to influence the work reported in this paper.

Data availability

Data will be made available on request.

Acknowledgments

The authors acknowledge to Adam Scannell for assisting with the hydro-thermal treatments and Rosalinda Inguanta for her valuable help in interpreting the XRD data.

References

Banivaheb, S., Ghalandari, V., Smith, H., Toufiq Reza, M., 2022. SolvX: Solvothermal Conversion of Mixed Waste Plastics in Supercritical Toluene in Presence of Pd/C Catalyst. J. Environ. Chem. Eng. 10 (6), 108622 https://doi.org/10.1016/j.jece.2022.108622.

Benavente, V., Fullana, A., Berge, N.D., 2017. Life Cycle Analysis of Hydrothermal Carbonization of Olive Mill Waste: Comparison with Current Management Approaches. J. Clean. Prod. 142 (January), 2637–2648. https://doi.org/10.1016/j.jclepro.2016.11.013.

Bermejo, M.D., Cocero, M.J., 2006. Supercritical Water Oxidation: A Technical Review. AIChE J 52 (11), 3933–3951. https://doi.org/10.1002/aic.10993.

Braden, J., Bai, X., 2018. Production of Biofuel Precursor Chemicals from the Mixture of Cellulose and Polyvinylchloride in Polar Aprotic Solvent. Waste Manag. 78 (August), 894–902. https://doi.org/10.1016/j.wasman.2018.07.011.

Braun, D., 2001. PVC — Origin, Growth, and Future. J. Vinyl Add. Tech. 7 (4), 168–176. https://doi.org/10.1002/vnl.10288.

Braun, D., 2002. Recycling of PVC. Prog. Polym. Sci. 27 (10), 2171–2195. https://doi.org/10.1016/S0079-6700(02)00036-9.

Burat, F., Güney, A., Olgaç Kangal, M., 2009. Selective Separation of Virgin and Post-Consumer Polymers (PET and PVC) by Flotation Method. Waste Manag. 29 (6), 1807–1813. https://doi.org/10.1016/j.wasman.2008.12.018.

Chen, G., Wang, X., Jiang, Y., Xindong, M.u., Liu, H., 2019. Insights into Deactivation Mechanism of Sulfonated Carbonaceous Solid Acids Probed by Cellulose Hydrolysis. Catal. Today, SI: Biomass Valorization 319 (January), 25–30. https://doi.org/10.1016/j.cattod.2018.03.069.

Corma, A., 1997. From Microporous to Mesoporous Molecular Sieve Materials and Their Use in Catalysis. Chem. Rev. 97 (6), 2373–2420. https://doi.org/10.1021/cr960406n.

Garcia, D., Balart, R., Crespo, J.E., Lopez, J., 2006. Mechanical Properties of Recycled PVC Blends with Styrenic Polymers. J. Appl. Polym. Sci. 101 (4), 2464–2471. https://doi.org/10.1002/app.23484.

Garcia, D., Balart, R., Sánchez, L., López, J., 2007. Compatibility of Recycled PVC/ABS Blends. Effect of Previous Degradation. Polym. Eng. Sci. 47 (6), 789–796. https://doi.org/10.1002/pen.20755.

Garlapalli, R.K., Wirth, B., Toufiq Reza, M., 2016. Pyrolysis of Hydrochar from Digestate: Effect of Hydrothermal Carbonization and Pyrolysis Temperatures on Pyrochar Formation. Bioresour. Technol. 220 (November), 168–174. https://doi.org/10.1016/j.biortech.2016.08.071.

Ghalandari, V., Banivaheb, S., Peterson, J., Smith, H., Toufiq Reza, M., 2022a. Solvothermal Liquefaction of Waste Polyurethane Using Supercritical Toluene in Presence of Noble Metal Catalysts. AIChE J. 68 (12), e17863.

Ghalandari, V., Smith, H., Volpe, M., Messineo, A., Reza, T., 2022b. Effect of Acidic Hydrochar on Plastic Crude Oil Produced from Hydrothermal Liquefaction of Waste PVC. Processes 10 (12), 2538. https://doi.org/10.3390/pr10122538.

Hongthong, S., Raikova, S., Leese, H.S., Chuck, C.J., 2020. Co-Processing of Common Plastics with Pistachio Hulls via Hydrothermal Liquefaction. Waste Manag. 102 (February), 351–361. https://doi.org/10.1016/j.wasman.2019.11.003.

Huang, N., Zhao, P., Ghosh, S., Fedyukhin, A., 2019. Co-Hydrothermal Carbonization of Polyvinyl Chloride and Moist Biomass to Remove Chlorine and Inorganics for Clean Fuel Production. Appl. Energy 240 (April), 882–892. https://doi.org/10.1016/j.apenergy.2019.02.050.

Jakab, E., Várhegyi, G., Faix, O., 2000. Thermal Decomposition of Polypropylene in the Presence of Wood-Derived Materials. J. Anal. Appl. Pyrol. 56 (2), 273–285. https://doi.org/10.1016/S0165-2370(00)00101-7.

Jiang, L.-b., Yuan, X.-Z., Li, H., Chen, X.-H., Xiao, Z.-H., Liang, J., Leng, L.-J., Guo, Z., Zeng, G.-M., 2016. Co-Pelletization of Sewage Sludge and Biomass: Thermogravimetric Analysis and Ash Deposits. Fuel Process. Technol. 145 (May), 109–115. https://doi.org/10.1016/j.fuproc.2016.01.027.

Kritzer, P., Dinjus, E., 2001. An Assessment of Supercritical Water Oxidation (SCWO): Existing Problems, Possible Solutions and New Reactor Concepts. Chem. Eng. J. 83 (3), 207–214. https://doi.org/10.1016/S1385-8947(00)00255-2.

Kuramochi, H., Nakajima, D., Goto, S., Sugita, K., Wei, W.u., Kawamoto, K., 2008. HCl Emission during Co-Pyrolysis of Demolition Wood with a Small Amount of PVC Film and the Effect of Wood Constituents on HCl Emission Reduction. Fuel 87 (13), 3155–3317. https://doi.org/10.1016/j.fuel.2008.03.021.

Lavric, E.D., Weyten, H., De Ruyck, J., Pleşu, V., Lavric, V., 2005. Delocalized Organic Pollutant Destruction through a Self-Sustaining Supercritical Water Oxidation Process. Energ. Conver. Manage. 46 (9), 1345–1364. https://doi.org/10.1016/j.enconman.2004.08.009.

Li, T., Zhao, P., Lei, M., Li, Z., 2017. Understanding Hydrothermal Dechlorination of PVC by Focusing on the Operating Conditions and Hydrochar Characteristics. Appl. Sci. 7 (3), 256. https://doi.org/10.3390/app7030256.

Lin, Y., Ma, X., Ning, X., Zhaosheng, Y.u., 2015. TGA–FTIR Analysis of Co-Combustion Characteristics of Paper Sludge and Oil-Palm Solid Wastes. Energ. Conver. Manage. 89 (January), 727–734. https://doi.org/10.1016/j.enconman.2014.10.042.

Lin, Y., Ma, X., Peng, X., Zhaosheng, Y.u., Fang, S., Lin, Y., Fan, Y., 2016. Combustion, Pyrolysis and Char CO2-Gasification Characteristics of Hydrothermal Carbonization Solid Fuel from Municipal Solid Wastes. Fuel 181 (October), 905–915. https://doi.org/10.1016/j.fuel.2016.05.031.

Lin, Y., Ge, Y.a., Xiao, H., He, Q., Wang, W., Chen, B., 2020. Investigation of Hydrothermal Co-Carbonization of Waste Textile with Waste Wood, Waste Paper and Waste Food from Typical Municipal Solid Wastes. Energy 210 (November), 118606. https://doi.org/10.1016/j.energy.2020.118606.

Liu, Z., Liu, Z., 2020. Comparison of Hydrochar- and Pyrochar-Based Solid Acid Catalysts from Cornstalk: Physiochemical Properties, Catalytic Activity and Deactivation Behavior. Bioresour. Technol. 297 (February), 122477 https://doi.org/10.1016/j.biortech.2019.122477.

Lu, J., Ma, S., Gao, J., 2002. Study on the Pressurized Hydrolysis Dechlorination of PVC. Energy Fuel 16 (5), 1251–2125. https://doi.org/10.1021/ef020048t.

Lu, X., Ma, X., Chen, X., Yao, Z., Zhang, C., 2020. Co-Hydrothermal Carbonization of Polyvinyl Chloride and Corncob for Clean Solid Fuel Production. Bioresour. Technol. 301 (April), 122763 https://doi.org/10.1016/j.biortech.2020.122763.

Ma, D., Feng, Q., Chen, B., Cheng, X.i., Chen, K., Li, J., 2019. Insight into Chlorine Evolution during Hydrothermal Carbonization of Medical Waste Model. J. Hazard. Mater. 380 (December), 120847 https://doi.org/10.1016/j.jhazmat.2019.120847.

Ma, S., Jun, L.u., Gao, J., 2002. Study of the Low Temperature Pyrolysis of PVC. Energy Fuel 16 (2), 338–342. https://doi.org/10.1021/ef0101053.

Ma, D., Liang, L., Erfeng, H.u., Chen, H., Wang, D., He, C., Feng, Q., 2021. Dechlorination of Polyvinyl Chloride by Hydrothermal Treatment with Cupric Ion. Process Saf. Environ. Prot. 146 (February), 108–117. https://doi.org/10.1016/j.psep.2020.08.040.

Ma, X., Liu, Y., Li, X., Jinguang, X.u., Guodong, G.u., Xia, C., 2015. Water: The Most Effective Solvent for Liquid-Phase Hydrodechlorination of Chlorophenols over Raney Ni Catalyst. Appl. Catal. B 165 (April), 351–439. https://doi.org/10.1016/j.apcatb.2014.10.035.

Nakamura, S., Nakajima, K., Yoshizawa, Y., Matsubae-Yokoyama, K., Nagasaka, T., 2009. Analyzing Polyvinyl Chloride in Japan With the Waste Input−Output Material Flow

Analysis Model. J. Ind. Ecol. 13 (5), 706–717. https://doi.org/10.1111/j.1530-9290.2009.00153.x.
Ning, X., Teng, H., Wang, G., Zhang, J., Zhang, N., Huang, C., Wang, C., 2020. Physiochemical, Structural and Combustion Properties of Hydrochar Obtained by Hydrothermal Carbonization of Waste Polyvinyl Chloride. Fuel 270 (June), 117526. https://doi.org/10.1016/j.fuel.2020.117526.
Patel, B., Guo, M., Izadpanah, A., Shah, N., Hellgardt, K., 2016. A Review on Hydrothermal Pre-Treatment Technologies and Environmental Profiles of Algal Biomass Processing. Bioresour. Technol., Pretreatment of Biomass 199 (January), 288–299. https://doi.org/10.1016/j.biortech.2015.09.064.
Patel, M.K., Jochem, E., Radgen, P., Worrell, E., 1998. Plastics Streams in Germany—an Analysis of Production, Consumption and Waste Generation. Resour. Conserv. Recycl. 24 (3), 191–215. https://doi.org/10.1016/S0921-3449(98)00015-9.
Patel, M., von Thienen, N., Jochem, E., Worrell, E., 2000. Recycling of Plastics in Germany. Resour. Conserv. Recycl. 29 (1), 65–90. https://doi.org/10.1016/S0921-3449(99)00058-0.
Pettersson, R.P., Olsson, M., 1998. A Nitric Acid-Hydrogen Peroxide Digestion Method for Trace Element Analysis of Milligram Amounts of Plankton and Periphyton by Total-Reflection X-Ray Fluorescence Spectrometry. J. Anal. At. Spectrom 13 (7), 609–613. https://doi.org/10.1039/A708575C.
Poerschmann, J., Weiner, B., Woszidlo, S., Koehler, R., Kopinke, F.-D., 2015. Hydrothermal Carbonization of Poly(Vinyl Chloride). Chemosphere 119 (January), 682–769. https://doi.org/10.1016/j.chemosphere.2014.07.058.
Pronobis, M., 2005. Evaluation of the Influence of Biomass Co-Combustion on Boiler Furnace Slagging by Means of Fusibility Correlations. Biomass Bioenergy 28 (4), 375–383. https://doi.org/10.1016/j.biombioe.2004.11.003.
Reza, M.T., Lynam, J.G., Helal Uddin, M., Coronella, C.J., 2013. Hydrothermal Carbonization: Fate of Inorganics. Biomass Bioenergy 49 (February), 86–94. https://doi.org/10.1016/j.biombioe.2012.12.004.
Sadat-Shojai, M., Bakhshandeh, G.-R., 2011. Recycling of PVC Wastes. Polym. Degrad. Stab. 96 (4), 404–415. https://doi.org/10.1016/j.polymdegradstab.2010.12.001.
Sato, Y., Kato, K., Takeshita, Y., Takahashi, K., Nishi, S., 1998. Decomposition of Ploy vinylchloride Using Supercritical Water. Jpn. J. Appl. Phys. 37 (11R), 6270. https://doi.org/10.1143/JJAP.37.6270.
Shen, Y., 2016. Dechlorination of Poly(Vinyl Chloride) Wastes via Hydrothermal Carbonization with Lignin for Clean Solid Fuel Production. Ind. Eng. Chem. Res. 55 (44), 11638–11644. https://doi.org/10.1021/acs.iecr.6b03365.
Slapak, M.J.P., van Kasteren, J.M.N., Drinkenburg, B.A.A.H., 1999. Hydrothermal Recycling of PVC in a Bubbling Fluidized Bed Reactor: The Influence of Bed Material and Temperature. Polym. Adv. Technol. 10 (10), 596–602. https://doi.org/10.1002/(SICI)1099-1581(199910)10:10<596::AID-PAT913>3.0.CO;2-J.
Sørum, L., Grønli, M.G., Hustad, J.E., 2001. Pyrolysis Characteristics and Kinetics of Municipal Solid Wastes. Fuel 80 (9), 1217–1227. https://doi.org/10.1016/S0016-2361(00)00218-0.
Tahmid, I.M., Saha, N., Hernandez, S., Klinger, J., Toufiq Reza, M., 2021a. Integration of Air Classification and Hydrothermal Carbonization to Enhance Energy Recovery of Corn Stover. Energies 14 (5), 1397. https://doi.org/10.3390/en14051397.
Tahmid, I.M., Sultana, A.I., Saha, N., Klinger, J.L., Toufiq Reza, M., 2021b. Pretreatment of Biomass by Selected Type-III Deep Eutectic Solvents and Evaluation of the Pretreatment Effects on Hydrothermal Carbonization. Ind. Eng. Chem. Res. 60 (43), 15479–15491. https://doi.org/10.1021/acs.iecr.1c03068.
Takeshita, Y., Kato, K., Takahashi, K., Sato, Y., Nishi, S., 2004. Basic Study on Treatment of Waste Polyvinyl Chloride Plastics by Hydrothermal Decomposition in Subcritical and Supercritical Regions. J. Supercrit. Fluids 31 (2), 185–193. https://doi.org/10.1016/j.supflu.2003.10.006.
Tekin, K., Karagöz, S., Bektaş, S., 2014. A Review of Hydrothermal Biomass Processing. Renew. Sustain. Energy Rev. 40 (December), 673–687. https://doi.org/10.1016/j.rser.2014.07.216.
Tortosa Masiá, A.A., Buhre, B.J.P., Gupta, R.P., Wall, T.F., 2007. Characterising Ash of Biomass and Waste. Fuel Process. Technol., Impacts of Fuel Quality on Power Production 88 (11), 1071–1081. https://doi.org/10.1016/j.fuproc.2007.06.011.
Uzoejinwa, B.B., He, X., Wang, S., Abomohra, A.-F., Yamin, H.u., Wang, Q., 2018. Co-Pyrolysis of Biomass and Waste Plastics as a Thermochemical Conversion Technology for High-Grade Biofuel Production: Recent Progress and Future Directions Elsewhere Worldwide. Energ. Conver. Manage. 163 (May), 468–492. https://doi.org/10.1016/j.enconman.2018.02.004.
Volpe, M., Messineo, A., Mäkelä, M., Barr, M.R., Volpe, R., Corrado, C., Fiori, L., 2020. Reactivity of Cellulose during Hydrothermal Carbonization of Lignocellulosic Biomass. Fuel Process. Technol. 206 (September), 106456 https://doi.org/10.1016/j.fuproc.2020.106456.
Volpe, M., Luz, F.C., Nepu Saha, M., Reza, T., Maryanne Chelang'at Mosonik, Roberto Volpe, and Antonio Messineo, 2021. Enhancement of Energy and Combustion Properties of Hydrochar via Citric Acid Catalysed Secondary Char Production. Biomass Convers. Biorefin., August. https://doi.org/10.1007/s13399-021-01816-z.
Wang, G., Zhang, J., Shao, J., Li, K., Zuo, H., 2015. Investigation of Non-Isothermal and Isothermal Gasification Process of Coal Char Using Different Kinetic Model. Int. J. Min. Sci. Technol. 25 (1), 15–21. https://doi.org/10.1016/j.ijmst.2014.11.012.
Wang, G., Zhang, J., Shao, J., Liu, Z., Zhang, G., Tao, X.u., Guo, J., Wang, H., Runsheng, X.u., Lin, H., 2016. Thermal Behavior and Kinetic Analysis of Co-Combustion of Waste Biomass/Low Rank Coal Blends. Energ. Conver. Manage. 124 (September), 414–426. https://doi.org/10.1016/j.enconman.2016.07.045.
Wang, Q.i., Zhang, J., Wang, G., Wang, H., Sun, M., 2018. Thermal and Kinetic Analysis of Coal with Different Waste Plastics (PVC) in Cocombustion. Energy Fuel 32 (2), 2145–2155. https://doi.org/10.1021/acs.energyfuels.7b03268.
Wei, Y., Fakudze, S., Yiming Zhang, R.u., Ma, Q.S., Chen, J., Liu, C., Chu, Q., 2022. Co-Hydrothermal Carbonization of Pomelo Peel and PVC for Production of Hydrochar Pellets with Enhanced Fuel Properties and Dechlorination. Energy 239 (January), 122350. https://doi.org/10.1016/j.energy.2021.122350.
Wu, X., Liang, J., Yulong, W.u., Husheng, H.u., Huang, S., Kejing, W.u., 2017. Co-Liquefaction of Microalgae and Polypropylene in Sub-/Super-Critical Water. RSC Adv. 7 (23), 13768–13776. https://doi.org/10.1039/C7RA01030C.
Xiu, F.-R., Yongwei, L.u., Qi, Y., 2020a. DEHP Degradation and Dechlorination of Polyvinyl Chloride Waste in Subcritical Water with Alkali and Ethanol: A Comparative Study. Chemosphere 249 (June), 126138. https://doi.org/10.1016/j.chemosphere.2020.126138.
Xiu, F.-R., Wang, Y., Xuan, Y.u., Li, Y., Yongwei, L.u., Zhou, K.e., He, J., Song, Z., Gao, X., 2020b. A Novel Safety Treatment Strategy of DEHP-Rich Flexible Polyvinyl Chloride Waste through Low-Temperature Critical Aqueous Ammonia Treatment. Sci. Total Environ. 708 (March), 134532 https://doi.org/10.1016/j.scitotenv.2019.134532.
Xiu, F.-R., Tan, X., Qi, Y., Wang, M., 2023. Treatment of DEHP-Rich PVC Waste in Subcritical Urine Wastewater: Efficient Dechlorination, Denitrification, Plasticizer Decomposition, and Preparation of High-Purity Phthalic Acid Crystals. J. Hazard. Mater. 441 (January), 129820 https://doi.org/10.1016/j.jhazmat.2022.129820.
Yao, Z., Ma, X., 2018. Characteristics of Co-Hydrothermal Carbonization on Polyvinyl Chloride Wastes with Bamboo. Bioresour. Technol. 247 (January), 302–309. https://doi.org/10.1016/j.biortech.2017.09.098.
Yarahmadi, N., Jakubowicz, I., Martinsson, L., 2003. PVC Floorings as Post-Consumer Products for Mechanical Recycling and Energy Recovery. Polym. Degrad. Stab. 79 (3), 439–448. https://doi.org/10.1016/S0141-3910(02)00360-9.
Yoshioka, T., Kameda, T., Imai, S., Noritsune, M., Okuwaki, A., 2008. Dechlorination of Poly(Vinylidene Chloride) in NaOH/Ethylene Glycol as a Function of NaOH Concentration, Temperature, and Solvent. Polym. Degrad. Stab. 93 (10), 1979–1984. https://doi.org/10.1016/j.polymdegradstab.2008.06.008.
Yu, J., Sun, L., Chuan Ma, Y.u., Qiao, and Hong Yao, 2016a. Thermal Degradation of PVC: A Review. Waste Manag. 48 (February), 300–314. https://doi.org/10.1016/j.wasman.2015.11.041.
Yu, L., Zhuang, X., Bai, L., Li, F., He, W., Li, G., Huang, J., 2016b. Acetic Acid Production from the Hydrothermal Transformation of Organics in Waste Liquid Crystal Display Panels. J. Clean. Prod. 113 (February), 925–930. https://doi.org/10.1016/j.jclepro.2015.11.056.
Zhang, X., Zhang, L., Li, A., 2019. Co-Hydrothermal Carbonization of Lignocellulosic Biomass and Waste Polyvinyl Chloride for High-Quality Solid Fuel Production: Hydrochar Properties and Its Combustion and Pyrolysis Behaviors. Bioresour. Technol. 294 (December), 122113 https://doi.org/10.1016/j.biortech.2019.122113.
Zhao, P., Li, Z., Li, T., Yan, W., Ge, S., 2017. The Study of Nickel Effect on the Hydrothermal Dechlorination of PVC. J. Clean. Prod. 152 (May), 38–46. https://doi.org/10.1016/j.jclepro.2017.03.101.
Zhao, P., Li, T., Yan, W., Yuan, L., 2018. Dechlorination of PVC Wastes by Hydrothermal Treatment Using Alkaline Additives. Environ. Technol. 39 (8), 977–985. https://doi.org/10.1080/09593330.2017.1317841.
Zhao, P., Huang, N., Li, J., Cui, X., 2020. Fate of Sodium and Chlorine during the Co-Hydrothermal Carbonization of High-Alkali Coal and Polyvinyl Chloride. Fuel Process. Technol. 199 (March), 106277 https://doi.org/10.1016/j.fuproc.2019.106277.
Zhao, Y., Jia, G., Shang, Y., Zhao, P., Cui, X., Guo, Q., 2022. Chlorine Migration during Hydrothermal Carbonization of Recycled Paper Wastes and Fuel Performance of Hydrochar. Process Saf. Environ. Prot. 158 (February), 495–502. https://doi.org/10.1016/j.psep.2021.12.041.
Zhao, D.i., Zhang, J., Wang, G., Conejo, A.N., Runsheng, X.u., Wang, H., Zhong, J., 2016. Structure Characteristics and Combustibility of Carbonaceous Materials from Blast Furnace Flue Dust. Appl. Therm. Eng. 108 (September), 1168–1177. https://doi.org/10.1016/j.applthermaleng.2016.08.020.
Zhou, H., Chunfei, W.u., Onwudili, J.A., Meng, A., Zhang, Y., Williams, P.T., 2015. Effect of Interactions of PVC and Biomass Components on the Formation of Polycyclic Aromatic Hydrocarbons (PAH) during Fast Co-Pyrolysis. RSC Adv. 5 (15), 11371–21137. https://doi.org/10.1039/C4RA10639C.
Zou, S., Yulong, W.u., Yang, M., Li, C., Tong, J., 2009. Thermochemical Catalytic Liquefaction of the Marine Microalgae Dunaliella Tertiolecta and Characterization of Bio-Oils. Energy Fuel 23 (7), 3753–4378. https://doi.org/10.1021/ef9000105.